Kinetics of random aggregation-fragmentation processes with multiple components

I. J. Laurenzi[1,*] and S. L. Diamond[2,†]

[1]*Department of Molecular Biophysics and Biochemistry, Yale University, P.O. Box 208114, New Haven, Connecticut 06520*

[2]*Department of Chemical Engineering, Institute for Medicine and Engineering, University of Pennsylvania, 3340 Smith Walk, Philadelphia, Pennsylvania 19104*

(Received 1 August 2002; published 9 May 2003)

A computationally efficient algorithm is presented for exact simulation of the stochastic time evolution of spatially homogeneous aggregation-fragmentation processes featuring multiple components or conservation laws. The algorithm can predict the average size and composition distributions of aggregating particles as well as their fluctuations, regardless of the functional form (e.g., composition dependence) of the aggregation or fragmentation kernels. Furthermore, it accurately predicts the complete time evolutions of all moments of the size and composition distributions, even for systems that exhibit gel transitions. We demonstrate the robustness and utility of the algorithm in case studies of linear and branched polymerization processes, the last of which is a two-component process. These simulation results provide the stochastic description of these processes and give new insights into their gel transitions, fluctuations, and long-time behavior when deterministic approaches to aggregation kinetics may not be reliable.

DOI: 10.1103/PhysRevE.67.051103 PACS number(s): 82.20.−w, 05.10.−a, 02.70.−c, 36.20.−r

I. INTRODUCTION

The aggregation of small entities into larger ones underlies processes as diverse as self-assembly, chemical polymerization, and blood coagulation. When aggregation is concurrent with fragmentation, many of these processes may be conceptualized as chemical polymerization processes,

$$M_i + M_j \underset{F(i,j)}{\overset{K(i,j)}{\rightleftharpoons}} M_{i+j}, \tag{1}$$

where M_i and M_j are particles of sizes i and j, and the aggregation and fragmentation kernels $K(i,j)$ and $F(i,j)$ function as ''chemical'' rate constants. The size dependencies of the kernels may be derived by the microphysical consideration of the mechanism of a given process. Hence, Eq. (1) is a general model by which many reversible aggregation processes may be represented.

As written, Eq. (1) describes a process with a single conservation law, i.e., conservation of monomers. However, aggregation and fragmentation processes may also feature additional conservation laws for other distinct monomeric units. For example, a detailed account of the kinetics of blood coagulation requires conservation laws for each active blood component: platelets, leukocytes, soluble fibrinogen, etc. To represent such processes, Eq. (1) must be modified to account for the additional conservation laws or components. Let us define each multicomponent species $M(\mathbf{u})$ by a composition vector $\mathbf{u}=(u_1,u_2,\ldots,u_\kappa)$, where u_k $(k\in[1,\kappa])$ is the amount of the kth conserved quantity or component. We may then rewrite Eq. (1) for this multicomponent or multiconservative model as

$$M(\mathbf{u}) + M(\mathbf{v}) \underset{F(\mathbf{u},\mathbf{v})}{\overset{K(\mathbf{u},\mathbf{v})}{\rightleftharpoons}} M(\mathbf{u}+\mathbf{v}). \tag{2}$$

In this case, $K(\mathbf{u},\mathbf{v})$ and $F(\mathbf{u},\mathbf{v})$ are multicomponent aggregation and fragmentation kernels that may depend on each component of $\mathbf{u}$ and $\mathbf{v}$.

To quantify the time evolution of aggregation-fragmentation processes, the kinetic process represented by Eq. (2) must be employed in a mathematical statement of component conservation. The traditional approaches of Smoluchowski [1], Blatz and Tobolsky [2], and Lushnikov [3] have achieved this by use of the deterministic population balance equations (PBEs) such as

$$\begin{aligned}\frac{\partial c(\mathbf{u},t)}{\partial t} = {} & \frac{1}{2}\sum_{\mathbf{v}=\mathbf{0}}^{\mathbf{u}} K(\mathbf{v},\mathbf{u}-\mathbf{v})c(\mathbf{v},t)c(\mathbf{u}-\mathbf{v},t) \\ & - \sum_{\mathbf{v}=\mathbf{0}}^{\infty} K(\mathbf{u},\mathbf{v})c(\mathbf{u},t)c(\mathbf{v},t) \\ & - \frac{1}{2}\sum_{\mathbf{v}=\mathbf{0}}^{\mathbf{u}} F(\mathbf{v},\mathbf{u}-\mathbf{v})c(\mathbf{u},t) + \sum_{\mathbf{v}=\mathbf{0}}^{\infty} F(\mathbf{u},\mathbf{v})c(\mathbf{u}+\mathbf{v},t).\end{aligned} \tag{3}$$

In this expression, $c(\mathbf{u},t)$ is the concentration of $\mathbf{u}$-mers and the sums are computed over each composition $\mathbf{v}=(v_1,v_2,\ldots,v_\kappa)\in\mathbb{N}^\kappa$, excluding the upper and lower limits.

Because PBEs, such as Eq. (3), are infinite sets of infinitely coupled nonlinear differential equations, obtaining their analytical and numerical solutions can be formidable challenges. Only a handful of analytical solutions of PBEs are known for processes with no fragmentation, most of

*FAX: (203) 432-5175.

Email address: laurenzi@bioinfo.mbb.yale.edu

†FAX: (215) 573-7227. Email address: sld@seas.upenn.edu

which are for single-component systems [1,3–8]. Furthermore, only two analytical solutions are known for single-component aggregation-fragmentation processes [2,9], and none are known for multicomponent aggregation-fragmentation processes. In addition, it has been shown that PBEs have validity only in the large population limit, that is, when there are many aggregates of each composition **u**. Consequently, PBEs cannot predict the long-time behaviors of aggregation processes when the particles or molecules completely aggregate or undergo a phase transition [10–12].

Owing to these considerations, the stochastic approach to aggregation kinetics has emerged as a viable and attractive alternative [10–20]. The stochastic approach can give a more realistic and robust characterization of aggregation processes, explicitly accounting for both the conservation of monomers and the statistical fluctuations of **u**-mer populations. In this paper, we employ this approach to exactly characterize the kinetics of reversible aggregation, wherein multiple components or conservation laws are extant. We then present an exact Monte Carlo (MC) algorithm for simulation of the time evolution of any spatially homogeneous aggregation process. The paper is organized as follows. In Sec. II, we derive the probability functions utilized by the MC algorithm, setting the stage for the presentation of the algorithm in Sec. III. We then apply the MC algorithm to study the kinetics of physically relevant reversible polymerization processes in Sec. IV. Here, we give the exact stochastic descriptions of the time evolutions of the linear (RA_g) and branched (RA_g/RB_2) models of reversible polymerizations of multivalent monomers, and develop methods of characterizing their gel points exactly. We conclude with a discussion of the results in Sec. V.

II. STOCHASTIC APPROACH

In a previous paper, we developed the stochastic formalism for the description of irreversible aggregation of particles with multiple components or conservation laws [12]. We summarize those results here and develop the additional details pertaining to particle fragmentation.

Consider a well-mixed and spatially homogeneous volume V in which there reside particles belonging to N distinct aggregate species, and let each species μ be characterized by a unique composition $\mathbf{u}_\mu=(u_{\mu,1},\ldots,u_{\mu,\kappa})$. That is, each particle having the composition $\mathbf{u}_\mu$ is a member of the μth species. After time $t=0$, these species will randomly aggregate or fragment according to the mechanism of Eq. (2), resulting in a change in the populations of one or more species. To specify these changes mathematically, we specify the state of the system by a vector $\mathbf{x}\equiv(X_1,\ldots,X_N)$, where X_μ is the population (number of particles) of the μth species. Subsequently, we specify the probabilities of aggregation and fragmentation of each species $\mu\in[1,N]$ in that state. Applying the stochastic approach to the chemical kinetics of the forward ''reaction'' of Eq. (2), one obtains the following transition probabilities for aggregation events [12,19]:

$$a(\mu,\nu)dt=V^{-1}K(\mathbf{u}_\mu,\mathbf{u}_\nu)X_\mu X_\nu dt$$
$$=\Pr(\text{any two particles of } \textit{unlike} \text{ species } \mu \text{ and } \nu \text{ with populations } X_\mu \text{ and } X_\nu \text{ will aggregate within the imminent time interval } dt), \quad (4)$$

$$a(\mu,\mu)dt=V^{-1}K(\mathbf{u}_\mu,\mathbf{u}_\mu)\frac{X_\mu(X_\mu-1)}{2}dt$$
$$=\Pr(\text{any two particles of the } \textit{same} \text{ species } \mu \text{ with population } X_\mu \text{ will aggregate within the imminent time interval } dt). \quad (5)$$

Applying the stochastic approach to the chemical kinetics of the reverse reaction of Eq. (2) likewise yields the following transition probabilities for fragmentation events:

$$f(\mu,\mathbf{v})dt=F(\mathbf{u}_\mu-\mathbf{v},\mathbf{v})X_\mu dt$$
$$=\Pr(\text{any particle of species } \mu \text{ with population } X_\mu \text{ and composition } \mathbf{u}_\mu \text{ will break into two unlike particles of compositions } \mathbf{u}_\mu-\mathbf{v} \text{ and } \mathbf{v} \text{ within the imminent time interval } dt), \quad (6)$$

$$f(\mu,\mathbf{u}_\mu)dt=\frac{1}{2}F\left(\frac{\mathbf{u}_\mu}{2},\frac{\mathbf{u}_\mu}{2}\right)X_\mu dt$$
$$=\Pr\Big(\text{any particle of species } \mu \text{ with population } X_\mu \text{ and composition } \mathbf{u}_\mu \text{ will break into two identical particles of composition } \frac{\mathbf{u}_\mu}{2} \text{ within the imminent time interval } dt. \quad (7)$$

In these definitions, the population terms enumerate the number of ways by which the reactant species can be chosen. For example, there are $X_\mu X_\nu$ ways that a pair of distinct species μ and ν can be chosen to aggregate. Likewise, there are X_μ ways of choosing a species μ for a fragmentation. The factor $\frac{1}{2}$ in Eq. (7) is a consequence of the fact that there is only one way that a particle can split in half, but two ways that it can be split asymmetrically.

In principle, **u**-mers may have many structural configurations, each with its own size or shape that may affect the rates of aggregation and fragmentation. However, neither the PBE nor our definition of species explicitly accounts for the configuration or shape. Consequently, it is possible that any **u**-mer particle may exhibit any of the $N(\mathbf{u})$ possible configurations of **u**-mers, regardless of the population of **u**-mers.

Thus, for Eqs. (4)–(7) to be generally valid for all aggregation-fragmentation processes, even for singly populated species, the kernels $K(\mathbf{u},\mathbf{v})$ and $F(\mathbf{u},\mathbf{v})$ must be the *average* rates of aggregation and fragmentation taken over all conformations, shapes, cross-sectional areas, and so forth. This condition implicitly requires that the conformation distributions of all species should remain constant throughout the aggregation process. In both the PBE and the stochastic approach to aggregation kinetics, this is commonly assumed to be true.

Using Eqs. (4)–(7), one can exactly derive probability distributions for both the event to come and the preceding quiescence time [12,19,21]. The probability that the imminent event will either be an aggregation of some species μ and ν or a fragmentation of some species μ into particles of compositions $\mathbf{v}$ and $\mathbf{u}_\mu-\mathbf{v}$ is

$$P_2(\mu,\nu;\mu,\mathbf{v}|\tau)=\begin{cases} f(\mu,\mathbf{v})/\alpha, & |\mathbf{v}|>0, \quad \nu=0 \\ a(\mu,\nu)/\alpha, & |\mathbf{v}|=0, \quad \mu,\nu>0, \end{cases} \tag{8}$$

where

$$\alpha=\sum_{\mu=1}^{N}(\alpha_\mu+X_\mu\phi_\mu) \tag{9}$$

is the sum of all transition frequencies $a(\mu,\nu)$ and $f(\mu,\mathbf{v})$, and

$$\alpha_\mu=\sum_{\nu=1}^{\mu}a(\mu,\nu) \tag{10}$$

and

$$\phi_\mu=\sum_{\mathbf{v}=0}^{[(1/2)\mathbf{u}_\mu]}F(\mathbf{u}_\mu-\mathbf{v},\mathbf{v}), \quad \mathbf{v}=(v_1,\ldots,v_\kappa) \tag{11}$$

are so defined for reasons that will become apparent later. The probability that the next event will occur immediately after the quiescence interval τ is

$$P_1(\tau)d\tau=\alpha P_0(\tau+t|t)d\tau, \tag{12}$$

where $P_0(t+\tau|t)$ is the probability that nothing will occur within the quiescence time. Because $\alpha\delta\tau$ is the probability that something will occur within the next time interval $\delta\tau$, it may be specified thus

$$P_0(t+\delta\tau|t)=P_0(t+0|t)[1-\alpha\delta\tau+O(\delta\tau)]. \tag{13}$$

By transposing $P_0(t+0|t)$ from the left-hand side of Eq. (13) and dividing throughout by $\delta\tau$ and letting $\delta\tau\to0$, one obtains the following differential equation for $P_0(t+\tau|t)$:

$$\frac{d}{d\tau}P_0(t+\tau|t)=\alpha P_0(t+\tau|t),$$

$$P_0(t+0|t)=1. \tag{14}$$

In the typical case where $K(\mathbf{u},\mathbf{v})$ and $F(\mathbf{u},\mathbf{v})$ are independent of time, the solution of Eq. (14) is

$$P_0(t+\tau|t)=\exp(-\alpha\tau). \tag{15}$$

However, if the aggregation and fragmentation kernels (and thus α) are explicit functions of time, Eq. (14) will yield a different expression for $P_0(t+\tau|t)$ and Eq. (8) should be evaluated at $t+\tau$. For example, time-dependent kernels may be necessary to describe the aggregations of biological cells, whose ability to adhere to each other is highly regulated and time dependent.

Because Eqs. (12) and (8) are derived analytically from Eqs. (4)–(7) without approximation, they are valid and exact for any process described by any set of aggregation and fragmentation kernels, regardless of their mathematical complexity or time dependence. Consequently, MC simulations based upon these formulas are tantamount to individual aggregation processes governed by kernels $K(\mathbf{u},\mathbf{v})$ and $F(\mathbf{u},\mathbf{v})$.

III. SIMULATION ALGORITHM

We now proceed to the development of the MC algorithm for reversible aggregation processes with multiple components. Fundamentally, the process of simulation entails three steps—the selection of the quiescence time preceding the imminent event, the selection of the event to come, and the modification of the state of the system to account for the occurrence of the chosen event. The process is then repeated until some predetermined time or, in the case of irreversible aggregation, the system is reduced to a single particle possessing all of the mass and other conserved quantities of the system.

The most computationally efficient method for the exact selection of the quiescence interval and event to come is a modified version of Gillespie's direct method [21]. In this method, random variables are selected by integrating their distributions until a uniform random number is just exceeded. Hence, the quiescence time is selected from Eq. (12) as follows [21]:

$$\int_0^\tau\alpha\exp(-\alpha\tau)d\tau=r_1, \quad r_1\in[0,1), \tag{16}$$

where r_1 is a uniform random number. Inverting this expression, one obtains an explicit equation for the quiescence time,

$$\tau=\frac{1}{\alpha}\ln\left(\frac{1}{1-r_1}\right), \quad \tau \text{ selection}. \tag{17}$$

Similarly, the imminent event is specified by summing over all $P_2(\mu,\nu;\mu,\mathbf{v}|\tau)$ until another uniform random number $r_2\in[0,1)$ is exceeded. That is, if the term $a(\mu,\nu)/\alpha$ causes the running sum of the terms of $P_2(\mu,\nu;\mu,\mathbf{v}|\tau)$ to exceed r_2, then the imminent event will be an aggregation of species μ and ν.

Unfortunately, a simple equation such as Eq. (17) cannot be written for the definition of the imminent event. However, the imminent event may be selected by judicious integration

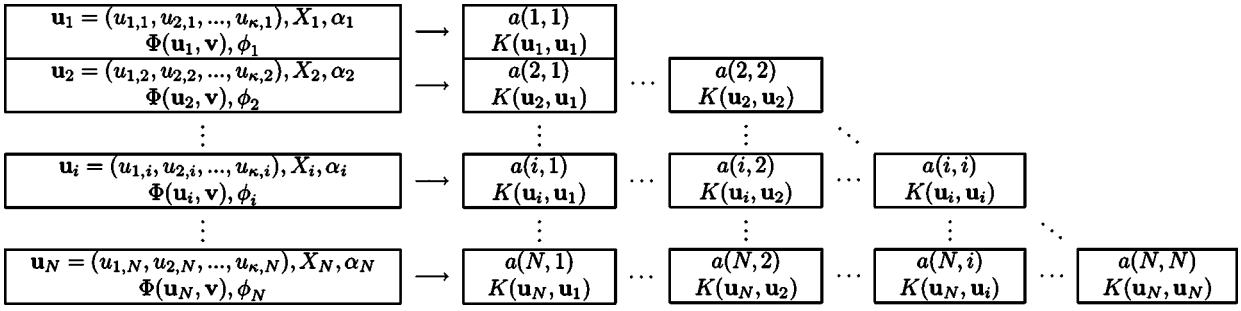

FIG. 1. Aggregation table for storing information pertaining to the state of the system and probabilities of aggregation and fragmentation events.

of Eq. (8). To begin with, we define the species μ involved in the imminent event by integrating over μ until the quantity $r_2\alpha$ is exceeded,

$$\sum_{i=1}^{\mu-1}(\alpha_i+X_i\phi_i)\leqslant r_2\alpha<\sum_{i=1}^{\mu}(\alpha_i+X_i\phi_i),\quad \mu \text{ selection.} \tag{18}$$

In this expression, we have employed the quantities α_i and ϕ_i defined by Eqs. (10) and (11). The choice between an aggregation or a fragmentation is implicitly specified during this process. If α_μ causes $r_2\alpha$ to be exceeded in Eq. (18), then the event to come is an aggregation of species μ with some other species; otherwise, the event to come will be a fragmentation,

$$\begin{aligned}&\sum_{i=1}^{\mu-1}(\alpha_i+X_i\phi_i)+\alpha_\mu>r_2\alpha,\quad \text{aggregation of species } \mu,\\ &\sum_{i=1}^{\mu-1}(\alpha_i+X_i\phi_i)+\alpha_\mu\leqslant r_2\alpha,\ \text{fragmentation of species } \mu.\end{aligned} \tag{19}$$

Finally, the imminent event is selected by determining which individual $a(\mathbf{u}_\mu,\mathbf{u}_\nu)$ or $f(\mathbf{u}_\mu,\mathbf{v})$ caused the sum of $P_2(\mu,\nu;\mu,\mathbf{v}|\tau)$ to exceed $r_2\alpha$ (18). If the imminent event is an aggregation, then the species index ν of the second particle is specified by

$$\begin{aligned}\sum_{j=1}^{\nu-1}a(\mu,j)\leqslant r_2\alpha-\sum_{i=1}^{\mu-1}(\alpha_i+X_i\phi_i)\\ <\sum_{j=1}^{\nu}a(\mu,j),\quad \nu \text{ selection,}\end{aligned} \tag{20}$$

where we note that the quantity $\Sigma_{i=1}^{\mu-1}(\alpha_i+X_i\phi_i)$ was previously calculated in the μ-selection step. Conversely, if the imminent event is a fragmentation, the composition $\mathbf{v}$ of the smaller daughter fragment of species μ is selected by summing the terms $f(\mathbf{u}_\mu,\mathbf{v})$ until the quantity $r_2\alpha-\Sigma_{i=1}^{\mu}\alpha_i-\Sigma_{i=1}^{\mu-1}X_i\phi_i$ is exceeded. Let us define the partial sum of fragmentation kernels by

$$\Phi(\mathbf{u}_\mu,\mathbf{v})=\sum_{\mathbf{w}=\mathbf{0}}^{[(1/2)\mathbf{v}]}F(\mathbf{u}_\mu,\mathbf{w}), \tag{21}$$

where $\Phi(\mathbf{u}_\mu,\mathbf{u}_\mu)=\phi_\mu$. The $\mathbf{v}$-selection criterion may then be written as

$$X_\mu\Phi(\mathbf{u}_\mu,\mathbf{v})>r_2\alpha-\sum_{i=1}^{\mu}\alpha_i-\sum_{i=1}^{\mu-1}X_i\phi_i,\quad \mathbf{v} \text{ selection,} \tag{22}$$

such that $\mathbf{v}$ is the first composition in the order of summation in Eq. (21) which causes the right-hand side (RHS) of Eq. (22) to be exceeded. In practice, this may be done by consecutive summation using Eq. (21) or by solving Eq. (22) by bisection when a simpler form of $\Phi(\mathbf{u}_\mu,\mathbf{v})$ is known analytically.

Given these rules for the MC selection of the quiescence time and imminent event, the following general simulation algorithm may be outlined.

(1) Initialize the process by defining all initial species and their properties [$\mathbf{u}_\mu$, X_μ, α_μ, ϕ_μ, $\Phi(\mathbf{u}_\mu,\mathbf{v})$, $K(\mathbf{u}_\mu,\mathbf{v})$, and $a(\mu,\nu)$] and compute α [Eq. (9)].

(2) Select the quiescence time [Eq. (17)] and the imminent event [Eqs. (18)–(22)].

(3) Increment the time by τ and modify the state of the system to account for the selected aggregation or fragmentation event.

(4) Recompute α. If $\alpha=0$, stop the simulation. Otherwise, return to step (2).

The computationally intensive aspects of this algorithm may be streamlined using an ''aggregation table'' (Fig. 1) as previously described [12]. The aggregation table is composed of an $N\times 1$ ''species vector'' containing information specific to each species [$\mathbf{u}_\mu$, X_μ, α_μ, ϕ_μ, and $\Phi(\mathbf{u}_\mu,\mathbf{v})$] and a lower-diagonal $N\times N$ ''aggregation matrix'' containing information specific to pairs of species [$K(\mathbf{u}_\mu,\mathbf{u}_\nu)$, $a(\mu,\nu)$]. This organization serves two functions: (a) facilitation of the creation, deletion, and update of species in steps (1) and (3), and (b) reduction of the number of computations necessary for the event and quiescence time selection steps.

In step (1), the state of the system is defined by successively adding each initial species to the bottom of the species vector and defining its corresponding row in the aggregation matrix. For each new species added to the bottom of the table (N), the composition $\mathbf{u}_N$ and population X_N are entered

first. Subsequently, the functions $\Phi(\mathbf{u}_N,\mathbf{v})$ are computed and stored, thereby defining ϕ_N. Finally, $\{a(N,i)\}$ and $\{K(\mathbf{u}_N,\mathbf{u}_i)\}(i\in[1,N])$ are added to the Nth row of the aggregation matrix, and α_N is computed according to Eq. (10). Due to the structure of the table, α_N is just the sum of the transition probabilities $a(N,i)$ in this row. Furthermore, α is just the sum of the quantities α_μ for each species μ in the species vector.

In the course of simulation, product particles resulting from an aggregation or fragmentation event will often have unique compositions and constitute new species. In such cases, these new species are added to the bottom of the aggregation table as discussed. However, if the product particle belongs to a species already represented in the species vector, the information for that species must be updated to reflect its change in population. The reactant species must likewise be updated. The aggregation table allows these modifications to be performed in a straightforward way. For example, consider a reactant or product species θ with population X_θ prior to the imminent event. First, the population of this species is incremented or decremented to reflect its generation or consumption. For example, if it aggregates with a species $\nu\neq\mu$, then the population is decremented by one. Subsequently, the quantities $\{a(\mu,i),i\in[1,\mu]\}$ and $\{a(j,\mu),j\in[\mu+1,N]\}$ in the μth row and μth column of the aggregation matrix are recomputed systematically using the colocally stored kernels $K(\mathbf{u}_\mu,\mathbf{v}_i)$ and $K(\mathbf{u}_j,\mathbf{v}_\mu)$. As these adjustments are made, the partial sums α_i $(i\geqslant\mu)$ are updated concurrently. Overall, this procedure requires $O(N)$ operations.

In processes featuring a gel transition or irreversible gelation, species are often completely consumed. In these cases, the procedure for updating the aggregation table is significantly simplified. Because the quantities $\{a(j,\mu),j\in[\mu+1,N]\}$ in the μth column of the aggregation matrix are recomputed with $X_\mu=0$, they will all be zero. Thus, the partial sums α_i $(j\in[\mu+1,N])$ only need to be decremented by the values $a(j,\mu)$ corresponding to the state *prior* to the event. Subsequently, the μth row of the aggregation table and μth column of the aggregation matrix may be deleted from computer memory without affecting the rest of the aggregation table. As a result, the memory usage of the algorithm is minimized.

A remarkable feature of the aggregation table and selection rules here presented is that the fragmentation transition frequencies $f(\mu,\mathbf{v})$ require neither direct computation nor storage. Here, the rationale underlying the definitions of ϕ_μ and $\Phi(\mathbf{u}_\mu,\mathbf{v})$ becomes apparent. Due to the fact that neither of these quantities are functions of X_μ, they require no adjustment once a species is initially defined. Consequently, the simulation procedure eliminates the extensive postevent accounting associated with the vast number of fragmentation transition probability densities $\{f(\mu,\mathbf{v})\}$ when species μ is a reactant or product. As a consequence, simulation of *any* reversible aggregation process is feasible regardless of the number of components. In simulations of strictly aggregating systems, computation of α and selection of a pair of aggregating particles require $O(N)$ operations per event [12]. When fragmentation is added to the simulation procedure as described and if the functions $\Phi(\mathbf{u}_\mu,\mathbf{v})$ for each species μ are stored in computer memory as lookup tables, only $O(\ln(N_{\max}))$ additional operations are required (refer to the Appendix). Consequently, the number of operations required of our algorithm per event is the same as that for the most efficient stochastic simulation algorithm for irreversible aggregation processes with multiple conservation laws or components [12]. Thus, simulations of nongelling aggregation-fragmentation processes with tens of thousands of particles typically require only seconds of central processing unit time to reach their steady states when run on a personal computer. However, processes that produce gels tend to be much more computationally demanding since they can require computation and storage of thousands of new fragmentation kernels after every event that involves the large, singly populated gel particle.

IV. KINETICS OF REVERSIBLE POLYMERIZATION

Polymerization is a specific type of aggregation process whereby the monomers are indistinguishable chemical entities. In many cases, these chemical monomers possess functional groups that can reversibly react with complementary groups attached to other monomers or polymers. In this section, we present MC simulation results for three such polymer models. We begin by considering the single-component linear polymerization model of Blatz and Tobolsky. We then consider single- and two-component processes that produce branched polymers.

Several features of these processes motivate the current study. First, the reaction-limited aggregation and fragmentation kernels may be computed exactly. Second, stationary composition distributions are known for these processes in the thermodynamic limit, and a transient solution of the PBE is known for the linear polymerization model [2,22]. Thus, simulation results can be compared against these distributions. Finally, the branched polymerizations have been theorized to exhibit gel transitions, defined by the rapid accumulation of a significant fraction of the system mass into a single particle. Our simulations may give insight into biological processes such as antibody agglutination and actin polymerization, which are characterized by similar branched polymerization mechanisms.

A. ARB model

The ARB process is named for its monomers that possess one A group and one B group apiece. Due to the chemical reaction

$$\mathrm{A}+\mathrm{B}\underset{k_2}{\overset{k_1}{\rightleftharpoons}}\mathrm{A}\text{—}\mathrm{B}, \tag{23}$$

the monomers bind to each other and give rise to linear polymers of the form ARB-$(\mathrm{ARB})_{k-2}$-ARB.

We concern ourselves with the reaction-limited process, where the particles collide much more frequently than they react. Hence, the rates of aggregation and fragmentation are

equal to the total rates of bond formation and dissociation. If internal cyclization is forbidden, every monomer and polymer chain will have one A group and one B group. Consequently, there will be two ways of attaching any two chains. If one further assumes equireactivity of all A and B groups, the total rate of bond formation between an *i*-mer and *j*-mer is

$$K(i,j)=2k_1. \tag{24}$$

The fragmentation kernel can be derived likewise by considering the number of ways that an $(i+j)$-mer can dissociate into an *i*-mer and a *j*-mer. As Eq. (23) shows, the rate of dissociation of any bond is k_2. Because an $(i+j)$-mer can lose an *i*-mer at either end, the total fragmentation rate is

$$F(i,j)=2k_2. \tag{25}$$

Note that both Eqs. (24) and (25) define constant kernels, that is, they exhibit no size dependence.

The kinetic time evolution of this process was first quantified by Blatz and Tobolsky, who solved a single-component PBE such as Eq. (3) with these kernels [2] and with a monodisperse initial condition $c(k,0)=c_0\delta_{k,1}$. Their solution for the time-dependent size distribution is

$$c(k,q)=c_0q^k(1-q)^2, \tag{26}$$

where c_0 is the initial concentration of monomers,

$$q=\frac{2}{(\lambda+2)+\sqrt{\lambda(\lambda+4)}\coth\left(\frac{1}{2}T\sqrt{\lambda(\lambda+4)}\right)}$$

is the extent of reaction of A or B groups, $\lambda=k_2/(k_1c_0)$ is the dimensionless dissociation constant, and $T=k_1c_0t$ is the dimensionless time.

To demonstrate the agreement of the stochastic method with the results of the PBE, simulations of the ARB polymerization process were simulated using 10 000 initial monomers ($c_0=1$, $V=1.0\times10^4$) at λ ranging over six orders of magnitude. We show the average results of sets of ten replicate simulations for $\lambda=1.0\times10^{-4}$ and $\lambda=1.0$ in Figs. 2 and 3, respectively. For all species with populations in excess of ten, the agreement between the average stochastic results and the deterministic results was excellent. However, differences between the approaches were evident for species with small populations. These differences are consequences of stochastic fluctuations of the populations of rare species, which cannot be predicted by deterministic approaches. In contrast, the populations of well-populated species are not strongly affected by these fluctuations. Thus, our results demonstrate that stochastic simulation can reproduce the time evolution of the size distribution as predicted by the PBE for a wide range of kernels, and provide insight regarding the statistical fluctuations of rare species.

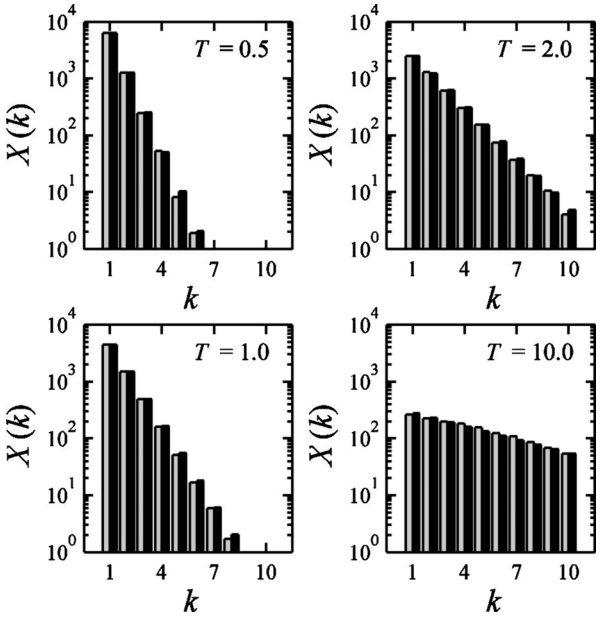

FIG. 2. Time evolution of the ARB polymerization process with $\lambda=1.0\times10^{-4}$. $X(k)$ is the number of *k*-mers at the dimensionless time *T*.

B. RA_g model

Unlike the process discussed in the preceding section, the RA_g process features monomers that have *g* A groups on each monomer. Moreover, these monomers aggregate as a result of the following chemical reaction between A groups on adjacent particles:

$$\mathrm{A}+\mathrm{A}\underset{k_2}{\overset{k_1}{\rightleftharpoons}}\mathrm{A}\text{—}\mathrm{A}. \tag{27}$$

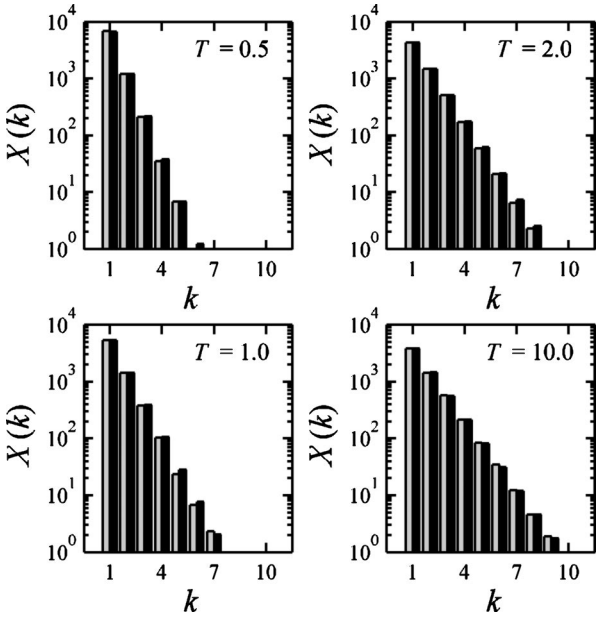

FIG. 3. Time evolution of the ARB polymerization process with $\lambda=1.0$. $X(k)$ is the number of *k*-mers at the dimensionless time *T*.

Hence, a 2-mer is composed of two RA_g monomers connected by an A—A bond, and has $2(g-1)$ A groups available to bind other monomers or aggregates.

The first quantitative study of the RA_g process was conducted by Stockmayer [22]. Assuming equireactivity of all A groups, forbidding internal cyclization (unbound A groups on an aggregate cannot react with each other), and assuming that the process begins with RA_g singlets alone, he obtained a stationary solution for the size distribution [22]

$$c(k,q)=c_0N_k(q/g)^{k-1}(1-q)^{\sigma_k(g)}, \tag{28}$$

where c_0 is the initial concentration of monomers, q is the extent of reaction of A groups,

$$\sigma_k(g)=(g-2)k+2 \tag{29}$$

is the number of free A groups on a k-mer, and

$$N_k=\frac{g^k(gk-k)!}{k!(\sigma_k(g))!} \tag{30}$$

is the number of unique structural isomers or configurations of acyclic k-mers. For example, one configuration is a linear chain, another has one branch, still another two branches, etc.

Stockmayer's distribution has interesting properties relating to gel transitions, whereat a significant portion of the monomers aggregate into a single particle. Stockmayer showed that if the conversion q reaches or exceeds a critical value q_c, the moments of Eq. (30) diverge for $n\geqslant 2$ and decrease for $n=1$. The first few moments

$$M_n(q)=\sum_{k=1}^{\infty} k^n c(k,q) \tag{31}$$

are

$$M_0(q)=c_0\left(1-\frac{g}{2}q\right), \tag{32}$$

$$M_1(q)=c_0 \quad q<q_c, \tag{33}$$

and

$$M_2(q)=c_0\frac{1+q}{1-(g-1)q}, \quad q<q_c, \tag{34}$$

representing the total concentration of particles (aggregates and singlets) in the system, the total concentration of monomers, and the width of the size distribution, respectively. Consequently, the thermodynamic analysis predicts a violation of monomer conservation and formation of an infinite particle at the gel point at the critical conversion,

$$q_c=\frac{1}{(g-1)}. \tag{35}$$

Although Stockmayer's solution is an exact result of thermodynamic analysis, it specifies neither the time evolution of the reversible RA_g polymerization, nor its gel point ($t=t_g$) at which q exceeds q_c. In theory, analytical solution of a PBE for this system could provide this information given valid kernels. However, such a solution has not been obtained explicitly. van Dongen and Ernst have estimated the time dependence of the reversible RA_g polymerization process using Ziff's method [23,24],

$$q(t)=\begin{cases}\dfrac{g(k_1c_0)t}{1+g(k_1c_0)t}, & \lambda=0\\[2ex] \dfrac{2q_\infty}{(1-q_\infty^2)\coth\left[\dfrac{1}{2}(k_1c_0)\kappa t\right]+(1+q_\infty^2)}, & \lambda>0.\end{cases} \tag{36}$$

In this expression, $q_\infty=(2g+\lambda-\kappa)/2g$ is the extent of reaction at steady state, $\lambda=k_2/(k_1c_0)$ is the dimensionless dissociation constant for the reaction between A groups, and $\kappa=[\lambda(\lambda+4g)]^{1/2}$. By equating this expression to q_c in the limit $t_g\to\infty$, one obtains the critical dimensionless equilibrium constant λ [24],

$$\lambda_c=\frac{g(g-2)^2}{(g-1)}, \tag{37}$$

above which gel transitions should not be observed.

Although Eq. (36) ascribes the time dependence to Stockmayer's distribution and the consumption of particles, it does not completely describe the time evolution of the RA_g polymerization process. Due to their radii of convergence, Eqs. (33) and (34) cannot be used to predict the time evolution of the higher-order moments of Stockmayer's distribution beyond the gel point. Alternative formulas for these moments have only been computed for the postgelation phase of the RA_3 polymerization [23], and neither these nor the preceding kinetic solution has been fully validated by substitution into the PBE or by comparison with stochastic simulation.

Stochastic simulations can predict the time course of the entire reversible RA_g polymerization process, regardless of whether gel transitions occur, as long as they are performed with proper kernels. The method of constructing kernels for polymerization processes was first developed by van Dongen and Ernst, and we summarize their results here. Following Stockmayer's assumptions of equireactivity of A groups, equal probabilities of all conformations of k-mers, and reaction-limited kinetics, the rate of aggregation will be equal to the average rate of bond formation between a pair of particles. Because there are $\sigma_i(g)\sigma_j(g)$ ways a bond may be formed between an i-mer and j-mer, the rate of bond formation between these particles is

$$K(i,j)=k_1\sigma_i(g)\sigma_j(g). \tag{38}$$

Because the fragmentation kernel is the average rate of breakup of a particle into two specific daughter fragments, the fragmentation kernel $F(i,j)$ is equal to the dissociation rate constant k_2 multiplied by the average number of ways that an $(i+j)$-mer can break into i-mers and j-mers. As discussed, there are two unique ways this can happen in a

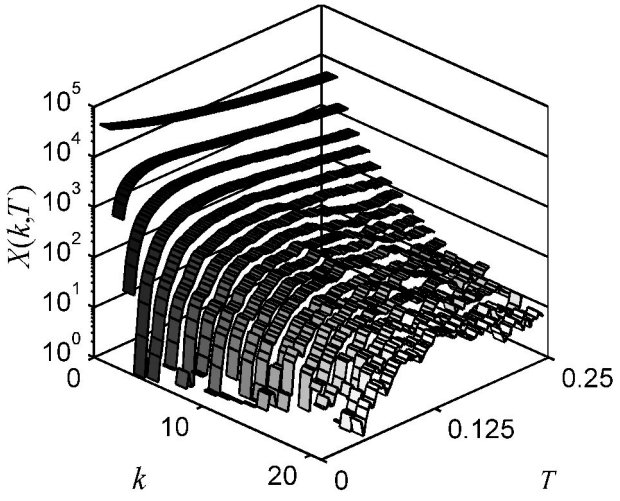

FIG. 4. Time evolution of the RA_3 polymerization process with $\lambda = 1/3$. $X(k,T)$ is the number of k-mers at the dimensionless time T.

linear polymerization ($g=2$), in which case the fragmentation kernel is $F(i,j)=2k_2$. However, in branched polymerizations an $(i+j)$-mer may be one of N_{i+j} unique structural configurations or structural isomers. In the absence of internal cyclization and if the initial size distribution is monodisperse, then the distribution of $(i+j)$-mers over their N_{i+j} configurations will be uniform [24]. Thus, the total number of ways that i-mers and j-mers of all configurations can be connected or disconnected is $\sigma_i(g)\sigma_j(g)N_iN_j$. Multiplying this combinatorial factor by the dissociation rate constant, one obtains the rate of dissociation of $(i+j)$-mers of all configurations into i-mers and j-mers. Since the rate of breakup must be equal to the rate of bond dissociation, this in turn must be exactly equal to the quantity $N_{i+j}F(i,j)$. Equating these quantities, one obtains the van Dongen and Ernst kernel [24]

$$F(i,j)=k_2\sigma_i(g)\sigma_j(g)\frac{N_iN_j}{N_{i+j}}. \tag{39}$$

Using these rate kernels, we simulated the RA_3 and RA_4 polymerization processes using 50 000 initial monomers ($c_0=1, V=5.0\times10^4$) at λ, above and below the critical values of λ_c for these two processes. We show these results in Figs. 4–8 in terms of a dimensionless time scale $T=c_0k_1t$.

In Fig. 4, we show the time evolution of the size distribution of an individual RA_4 polymerization simulation with $\lambda = \frac{1}{3}$ (gelling). In this figure, $X(k,T)$ [$=Vc(k,T)$] is the k-mer population at the dimensionless time T. Like the deterministic description, MC simulation predicted the diminishing populations of all k-mers after the gel point as these species were consumed by the gel. Additionally, stochastic simulation demonstrated the probabilistic character of the dynamics of k-mers as $X(k,T)\to1$. As we have discussed, strong fluctuations and a slight offset from the deterministic description are observed for small $X(k,T)$, particularly when $\lambda<\lambda_c$. Despite these fluctuations, the dynamic MC-generated size distribution of Fig. 4 cannot be distinguished from Eq. (28) by the χ^2 test. However, we note that p values for these tests were as low as 0.1 at some time points prior to the steady state.

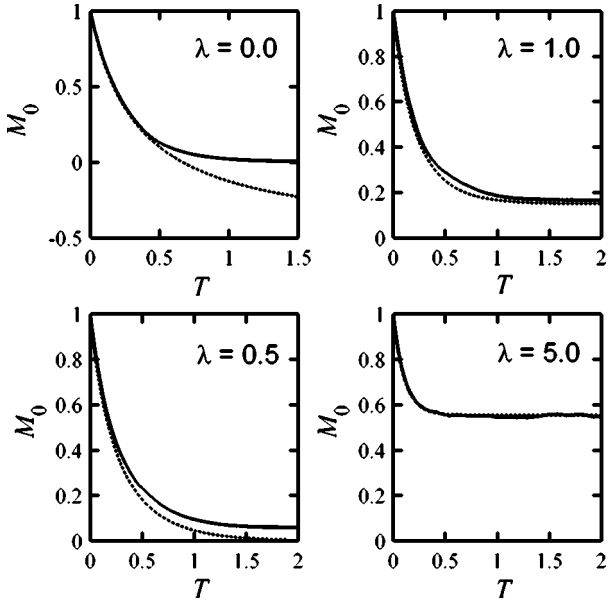

FIG. 5. Consumption of the number of particles (M_0) in RA_4 polymerization processes with various dissociation constants λ. Solid lines are simulation results, and dashed lines are results from the deterministic theory. Stochastic simulation always predicts positive numbers of particles and proper equilibria, even when $\lambda\leqslant\frac{1}{2}$.

In Figs. 5 and 6, we show how the average values of M_0 and M_2 evolve over time in stochastic simulation. The average values reported here were computed using the results of

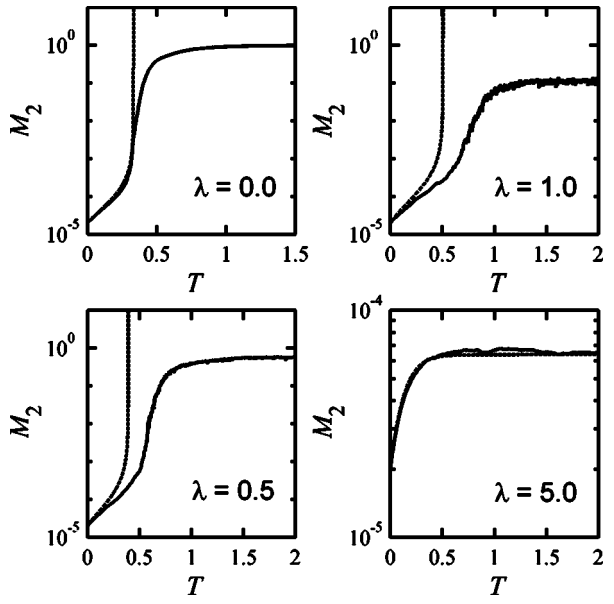

FIG. 6. Average widths of the RA_4 size distribution with various dissociation constants λ. Solid lines are simulation results, and dashed lines are results from the deterministic theory. Below the critical dissociation constant $\lambda_c=1/3$, systems of particles exhibit a gel transition. Stochastic simulation permits exact quantitation of the process in the postgel phase.

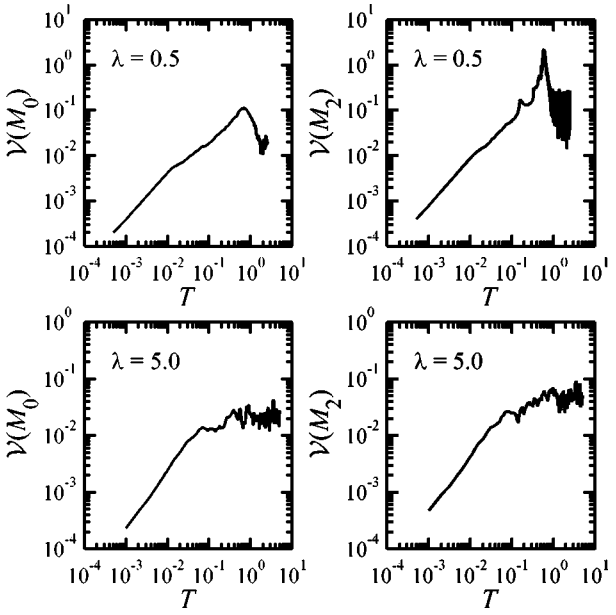

FIG. 7. Coefficients of variation of the zeroth and second moments of the RA_4 size distributions with dissociation constants in the gelling and nongelling regions. Peaks are observed only for processes that undergo a gel transition. Note that the coefficients of variation exceed unity in these cases, indicating strong fluctuations in the size distribution.

ten replicate simulations. We also show the deterministic predictions for comparison. We have normalized our results in accordance with the physical criterion,

$$\frac{[VM_k(t)]}{[VM_1(t)]^k} \leqslant 1, \quad k \geqslant 2, \tag{40}$$

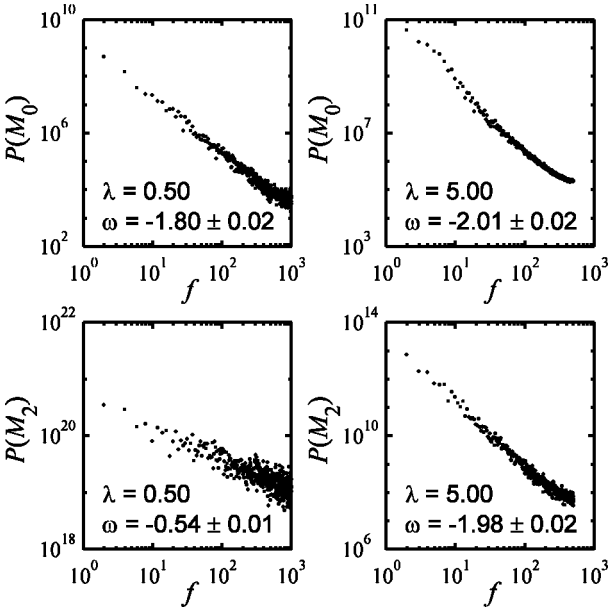

FIG. 8. Average power spectra of the zeroth and second moments of the RA_4 size distributions. The second moment has Brownian noise (slope ~ 2) for nongelling processes, but colored noise (slope <2) for gelling processes.

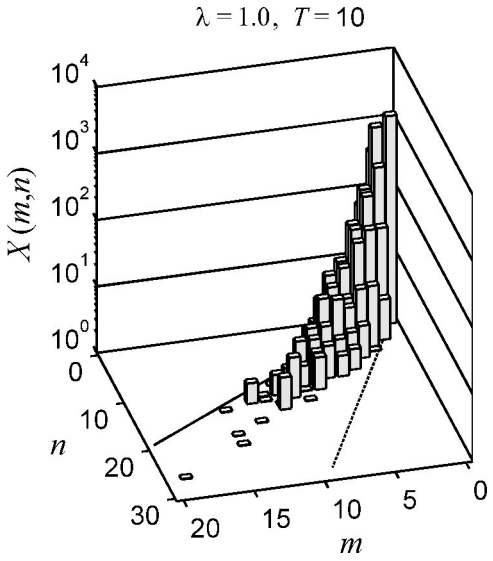

FIG. 9. Equilibrium RA_4/RB_2 particle composition distribution with dissociation constant $\lambda = 1$ and relative RA_4 monomer content $y = 0.4$. $X(m,n)$ is the number of particles composed of $m RA_4$ monomers and $n RB_2$ monomers. The dashed and solid lines are boundaries reflecting that aggregates must have more than zero free A and B groups, respectively.

which is true for all single-component aggregations of finite numbers of particles [3]. As we have mentioned, the deterministic equations predict a divergence of M_2 and a decrease in M_1 at the gel point, whereas the stochastic simulations predicts a rapid but finite increase in M_2 and rigorous conservation of mass. Just as noteworthy, however, are the differences between the predictions of the two approaches for time evolution of the total number of particles M_0. For all values of λ, stochastic simulations predicting a asymptotic decay of M_0 to a final positive value. However, when $\lambda \leqslant \frac{1}{2}$ the deterministic equations predict that M_0 will either vanish or become negative as $T \to \infty$. However, because M_0 is the total concentration of particles in the system, it cannot be negative. Hence, the deterministic equations fail, $\lambda \leqslant \frac{1}{2}$. As λ is increased, the agreement between the two approaches improves. For example, simulation results for M_0 with $\lambda = 1$ ($\lambda_c = 1.5$) are in fairly good agreement with the deterministic predictions, despite small differences in the decay rate after $T \simeq 0.3$ and a slight offset between the steady-state values. At $\lambda = 5$, both the stochastic and the deterministic predictions of the time evolutions of the zeroth and second moments are in close agreement.

Upon closer examination, it may be shown that the differences between the stochastic and the deterministic results are neither a consequence of a difference between the stochastic and the deterministic approaches to the kinetics of Eq. (27) [25,26], nor do they result from an error in Stockmayer's distribution. Rather, these differences and the deterministic prediction of negative zeroth moments primarily result from the assumptions underlying the kinetic derivation of Eq. (36) for $q(t)$. Equation (36) is derived by applying deterministic rate equations to Eq. (27) and assuming that all unbound A groups are free to react with all other unbound A groups [23,24]. However, the derivations of both Stockmayer's dis-

tribution and the kernels we have used forbid internal cyclization. Thus, any process starting with $X_0\mathrm{RA}_g$ monomers must have at least $\sigma_{X_0}(g)$ free A groups at any given time–the number possessed by a single aggregate of all RA_g monomers. This corresponds to a maximum extent of reaction

$$q_{\max}=[gX_0-\sigma_{X_0}(g)]/gX_0\simeq 2/g. \tag{41}$$

Because Eq. (36) neglects these considerations, it allows q to exceed $q_{\max}$ when λ is sufficiently small. When this occurs, Eq. (32) predicts that the number of particles in the system becomes negative. In summary, Eq. (36) is predictive for small T and for equilibrium constants in excess of λ_c, when extents of reaction are smaller than $q_{\max}$. However, it becomes progressively unreliable for values of λ smaller than λ_c. This is the reason why χ^2 testing of the simulation results shown in Fig. 4 yielded small p values for distributions at certain time points.

In addition to showing the deterministic and stochastic predictions for the time evolution of M_2 prior to gelation, Fig. 6 also shows the exact predictions of the time evolution of M_2 after the gel point. The shortcomings of Eq. (36) aside, deterministic approaches cannot predict the time evolution of the second moment beyond the gel point because Eq. (34) diverges as $q\rightarrow q_c$. Moreover, even their steady-state behavior is not guaranteed to obey Eq. (40) due to statistical factors lacking in Stockmayer's methodology and in the PBE [11,12]. However, any stochastic simulation of the aggregation of finite numbers of particles, even *moles* of particles, will predict size distributions with that obey Eq. (40) for all λ and reach a steady state.

The erroneous small λ behavior of Eq. (36) causes additional significant differences between the simulation results and the deterministic equations. Early in the aggregation process, both the deterministic and the stochastic approaches give equivalent predictions of the growth of M_2 because Eq. (36) predicts very small values of q. However, as Eq. (36) predicts values of q that approach $q_{\max}$, it begins to lose predictive power. This translates to small deviations in M_0 prior to the gel point ($q_c<q_{\max}$) because Eq. (32) predicts a linear relationship between q and M_0. However, the form of Eq. (34) enhances these deviations significantly. In fact, if the values of q given by Eq. (36) are decreased by approximately 10 time series for $\lambda=0.5$ and $\lambda=1.0$ agree very well prior to the gel point. In the irreversible ($\lambda=0$) and nongelling ($\lambda=5$) processes, there is a good agreement between simulation results and the deterministic equations. In the first case, the gel transition occurs before the shortcomings of Eq. (36) become evident. In the second case, Eq. (36) never predicts a conversion as large as $q_c(q_c<q_{\max})$, precluding the ''depletion'' of A groups for reaction that is its source of error.

A major consequence of this observation is that Eq. (36) cannot be used to accurately predict the gel point for the RA_g polymerization. However, stochastic simulation can characterize the gel point exactly. Since Eq. (32) is valid for all q, even in the stochastic approach, t_g is the time at which the average value of M_0 is equal to the value predicted by Eq. (32) with $q=q_c$. We will use this method to characterize the copolymerization process discussed in the following section. Interestingly, our simulation results and Eq. (37) agree in their predictions of the critical equilibrium constant λ_c for the RA_2, RA_3, and RA_4 polymerizations. Because $q_c<q_{\max}$, the aforementioned shortcomings of Eq. (36) do not appear to strongly influence the *steady-state* values of Eq. (36) on which Eq. (37) is based. Thus, our results suggest that the methodology used by van Dongen and Ernst to determine Eq. (37) is valid, even though Eq. (36) is not generally reliable.

In addition to allowing exact computation of the average moments and the gel point, stochastic simulation permits one to compute additional fluctuation statistics. In Fig. 7, we present respresentative results for the time evolutions of coefficients of variation ($\mathcal{V}$) for M_0 and M_2, for one gelling ($\lambda=0.2$) and one nongelling ($\lambda=0.2$) system. Like the average values of M_0 and M_2 presented in Figs. 5–6, the coefficients of variation presented in Fig. 7 were computed from the results of ten simulations. At $t=0$, the $\mathcal{V}(M_0)$ and $\mathcal{V}(M_2)$ are exactly zero since the initial condition is exactly known. Subsequently, these quantities rise as a result of the random generation and consumption of new species and the stochastic evolutions of their populations. The time evolutions of $\mathcal{V}(M_0)$ and $\mathcal{V}(M_2)$ have behaviors that distinguish gelling and nongelling systems. In nongelling processes, the coefficients of variation of both moments grow monotonically and approach asymptotic values that are always less than 1. However, the time evolutions of $\mathcal{V}(M_0)$ and $\mathcal{V}(M_2)$ are significantly different for gelling systems. If $\lambda<\lambda_c$, the time series of both $\mathcal{V}(M_0)$ and $\mathcal{V}(M_2)$ go through maxima prior to their steady states. Moreover, the time series of $\mathcal{V}(M_2)$ possesses a cusp at which $\mathcal{V}(M_2)$ exceeds unity, implying that the standard deviation of the gel size is greater than its average and this point is close to if not colocal with the gel point. These intense fluctuations have ramifications for the deterministic desciption of gelling systems, inasmuch as they relate to statistical terms usually neglected from the RHS of PBEs such as Eq. (3) [11,13]. For all reversible branched aggregation processes studied, a coefficient of variation for M_2 in excess of unity implied a gel transition. Finally, the steady-state values of $\mathcal{V}(M_2)$ are always much larger for gelling systems than the nongelling systems, whereas those for $\mathcal{V}(M_2)$ are relatively insensitive to λ or gelation.

The special behavior of the time evolutions of $\mathcal{V}(M_2)$ for gelling processes is a direct consequence of the properties of the gel. The gel size fluctuates rapidly because the gel is a single particle subject to random aggregations with other particles. However, unlike other singly populated species, the gel possesses a significant fraction of the monomers. Thus, a single random fragmentation of a gel can bring about a significant drop in M_2, whereas a population change in 1-mers from 1 to 0 will have little effect. Likewise, a random aggregation of singly populated large particles or gel ''daughters'' will result in large and immediate increases in M_2. The net result is that the steady state $\mathcal{V}(M_2)$ is much larger for gelling systems than for nongelling systems. In contrast, these

events have little effect upon $\mathcal{V}(M_0)$ because no single event can change M_0 by more than one.

In Figs. 6 and 7, both the average value and the coefficient of variation of M_2 appear to fluctuate after the gel transition, despite being statistical quantities taken from the results of ten replicate simulations. These fluctuations result from the fact that these statistics are computed from the results of only ten simulations. Because the gel is a single particle, the apparent fluctuations of the average and the coefficient of variation result from the considerable variation of the size of a gel from simulation to simulation (or experiment to experiment) at time t. To smooth out these apparent fluctuations, one must compute the statistics of M_2 using many more experiments or simulations. These fluctuations are not results of chaos or instability, and are not incompatible with the definitions of equilibrium and steady state.

Using spectral analysis, the steady states of the time series of the simulated size distributions and their moments can be shown to be proper equilibrium states. In Fig. 8, we show the average results of ten power spectra of $M_0(t)$ and $M_2(t)$ obtained by fast Fourier transform of their steady-state time series. The individual spectra could be statistically distinguished from the mean, thus, we conclude that the RA_g polymerization as simulated is ergodic. Moreover, the absence of distinct peaks in the spectra demonstrates an absence of periodic fluctuations at equilibrium. Similar results were obtained for simulation results of the RA_3 and RA_4 polymerizations over broad ranges of λ.

In addition, the power spectra of both moments have the form $P(f) \propto 1/f^{\omega}$, regardless of the values of λ and g used in the simulations, permitting a quantitative characterization of the fluctuations. A completely random signal is often denoted as ''white noise'' and has $\omega \simeq 0$, whereas processes such as Brownian motion produce signals with $\omega \simeq 2$. The ''noise'' associated with M_0 and M_2 depends upon the value of λ. When $\lambda > \lambda_c$, the noise of both moments is Brownian, that is, $\omega \simeq 2$. However, as λ decreases below λ_c, so does ω, resulting in what is often denoted as ''colored noise.'' Like the height of the peaks of the coefficients of variation in Fig. 7, the dependence of ω upon the equilibrium constant λ is much stronger for the second moment than for the zeroth moment. For an RA_3 polymerization with $\lambda = 0.5 (\lambda_c = 1.5)$, the exponent for the zeroth moment is about 1.8, which is essentially Brownian. In contrast, the exponent for the power spectrum of the second moment under these conditions is 0.54. Similar results are observed for all RA_g polymerizations except when $g=2$, where gelation cannot occur and $\omega \simeq 2$ for all λ. The power spectra of the zeroth moments of RA_g polymerizations have exponents that do not deviate substantially from 2, whereas the exponents from the second moment power spectra become smaller than 1 as λ is decreased below λ_c.

C. RA_g/RB_2 model

Like the RA_g process, the RA_g/RB_2 process is a polymerization that can produce highly branched aggregates. The RA_g/RB_2 process is a copolymerization of two types of monomers: one with g A groups and the other with two B groups. Hence, this process is a two-component system with conservation laws for each type of monomer. Like the single-component ARB polymerization, aggregation occurs via the bonding between A groups on RA_g monomers and B groups on RB_2 monomers as in Eq. (23). Thus, if one of the two types of monomers is absent, no polymerization can occur.

This process is analogous to the polymerization of antibodies (RB_2) with multivalent antigens (RA_g). In this case, the B groups are antigen-binding F_{ab} domains and the A groups are the corresponding multivalent antigenic determinants (epitopes). Hence, the RA_g/RB_2 model quantifies the kinetics of polymerization of bivalent antibodies (IgD, IgE, IgG, where Ig is immunoglobin) with polyvalent antigens. Likewise, the RA_g/RB_2 model describes the branched polymerization of polyfunctional antibodies such as IgM ($g=10$) or IgA ($g=4$) with antigens possessing two epitopes. The predisposition of an RA_g/RB_2 polymerization to form branched aggregates depends upon how many of the RB_2 and RA_g monomers are present initially.

Under the assumptions of equireactivity of A and B groups, no internal cyclization, and reaction-limited polymerization, Stockmayer calculated a stationary distribution for this process [22], which may be written as

$$c(\mathbf{u},q) = c_0 \frac{2g(1-q)(1-rq)}{q(2r+g)} \xi^m \zeta^n N(\mathbf{u}), \quad c_0 = c_{1,0} + c_{0,1}. \tag{42}$$

Here, m and n are the amounts of RA_g and RB_2 monomers in a $\mathbf{u}$-mer $[\mathbf{u}=(m,n)]$. Additionally, $c_{1,0}$ and $c_{0,1}$ are the total concentrations of RA_g and RB_2 monomers, respectively,

$$r = \frac{g c_{1,0}}{2 c_{0,1}} \tag{43}$$

is the ratio of A groups to B groups, q is the fractional extent of reaction of A groups, and the quantities ξ and ζ have been defined by Stockmayer in terms of q, g, and r [22]. The quantity

$$N(\mathbf{u}) = \frac{g^m 2^n (gm-m)!}{[A(\mathbf{u},g)]![B(\mathbf{u},g)]!m!}, \quad \mathbf{u}=(m,n) \tag{44}$$

is the number of unique structural isomers of a $\mathbf{u}$-mer, where the quantities

$$A(\mathbf{u},g) = (g-1)m - n + 1 \tag{45}$$

and

$$B(\mathbf{u},g) = n - m + 1 \tag{46}$$

are the number of free A and B groups on a $\mathbf{u}$-mer, respectively.

The moments of Eq. (42)

$$M_{k,\ell}(q) = \sum_{m=0}^{\infty} \sum_{n=0}^{\infty} m^k n^{\ell} c(\mathbf{u},q), \quad c((0,0),q) \equiv 0 \tag{47}$$

have physical interpretations similar to those of the moments discussed in the preceding section. However, their computation is not trivial except for the first moments $M_{1,0}=c_{1,0}$ and $M_{0,1}=c_{0,1}$, and the zeroth moment

$$M_{0,0}(p)=c_0(1-gqy), \quad q\in[0,\min((gy)^{-1},1)], \quad (48)$$

where

$$y=\frac{c_{1,0}}{c_0}=\left(\frac{2r}{2r+g}\right) \quad (49)$$

is the relative ratio of RA_g monomers to the total number of reactive monomers. Physically, the moments $M_{0,0}$, $M_{1,0}$, and $M_{0,1}$ are the total concentration of particles (singlets and aggregates), total concentration of RA_g, monomers and total concentration of RB_2 monomers, respectively. The second moments $M_{0,2}$, $M_{1,1}$, and $M_{2,0}$ are the widths of the distribution in RA_g and RB_2 composition. The mixed second moment $M_{1,1}$ indicates the extent of mixing of the two types of monomers in the aggregates. In analogy with the stationary distribution for the RA_g polymerization, these higher-order moments $(k+\ell\geqslant 2)$ will diverge when the conversion q exceeds the critical value

$$q_c=\frac{1}{\sqrt{r(g-1)}} \quad (50)$$

at the gel point t_g.

Although Stockmayer's description predicts conversion of a stationary system, it does not predict the time evolution of the RA_g/RB_2 process. Moreover, the gel criterion (50) does not specify whether or not a system will possess a gel transition for a specific combination of dimensionless chemical equilibrium constant $\lambda=k_2/(k_1c_0)$ and r (or y). As we have shown in the preceding section, the deterministic treatment of the kinetics of reactions such as Eq. (23) to ascribe the time dependence to the conversion q may not be reliable. Thus, we conducted stochastic simulations to characterize the kinetic time evolution of this process exactly and determine the λ and y dependencies of its gel point.

The derivations of the kernels for this process are analogous to those of the model of the preceding section. Again, we impose the constraints of (1) equireactivity of A and B groups, (2) reaction-limited aggregation, and (3) no internal cyclization. To define the aggregation kernel, the rate constant k_1 in Eq. (23) must be multiplied by the total number of ways of forming a bond between a **u**-mer and a **v**-mer. Enumerating the ways in which one can form a bond between A and B groups on these species, one obtains

$$K(\mathbf{u},\mathbf{v})=k_1[A(\mathbf{u},g)B(\mathbf{v},g)+A(\mathbf{v},g)B(\mathbf{u},g)]. \quad (51)$$

Note that if a combination of free A and B groups is not possible between these species, the aggregation kernel will be zero. For example, if $\mathbf{u}=\mathbf{v}=(1,0)$ (interaction of two RA_g monomers), both $B(\mathbf{u},g)$ and $B(\mathbf{v},g)$ will be zero on the RHS of Eq. (51). Employing the arguments of the preceding section, the fragmentation kernel may be written as

$$F(\mathbf{u},\mathbf{v})=k_2[A(\mathbf{u},g)B(\mathbf{v},g)+A(\mathbf{v},g)B(\mathbf{u},g)]\frac{N(\mathbf{u})N(\mathbf{v})}{N(\mathbf{u}+\mathbf{v})}, \quad (52)$$

where the combinatorial terms $N(\mathbf{u})$ are given by Eq. (44). Like the aggregation kernel, the fragmentation kernel accounts for the connectivity of A and B groups. If a composition **u** is inconsistent with the requirement that aggregates must be linked by A-B bonds, either $N(\mathbf{u})$ or $N(\mathbf{v})$ will be zero. Consequently, the fragmentation kernel does not permit the breakup of an $(\mathbf{u}+\mathbf{v})$-mer into daughter fragments that violate the chemistry and stoichiometry of Eq. (23).

Using these kernels, we conducted stochastic simulations for the RA_4/RB_2 system with 10 000 particles ($c_0=1.0$, $V=10\,000$) over broad ranges of y and λ. The valency was specifically chosen to represent the polymerization of an IgA antibody ($g=4$) with a bivalent antigen (two epitopes).

Figure 9 shows the complete steady-state ($T=10$) two-component size-composition distribution from a single simulation of an RA_4/RB_2 process with $y=0.5$ and $\lambda=1$. Like the process discussed in the preceding section, the steady states of this model constitute proper equilibria, since the time and data averages are equivalent in the limit of large t. Note that all the species conform to the aforementioned constraints $A(\mathbf{u},g)\geqslant 0$ (dashed line) and $B(\mathbf{u},g)\geqslant 0$ (solid line), reflecting the fact that the simulation algorithm cannot select an event having a zero kernel. Also, note that there is no gel in this distribution.

The absence of a gel in Fig. 9 (i.e., a large particle constituting a significant portion of the monomers) suggests via Eq. (50) that the equilibrium extent of reaction $q(\infty)$ is less than q_c. This hypothesis may be validated directly using Eq. (48) that, like Eq. (32), is exact in both the stochastic and the deterministic approaches. The composition distribution shown in Fig. 9 has $M_{0,0}(\infty)=3650$ particles, corresponding to a conversion $q(\infty)=0.397$. Stockmayer's gel criterion specifies that a conversion of $q_c=0.5$ is required for gelation, thus both the stochastic and the deterministic approaches agree that no gel transition occurs. Moreover, Eq. (42) with $q=0.397$ is indistinguishable from the composition distributions generated by stochastic simulation according to χ^2 significance testing ($p=1.0$).

Like the second moments of the size distribution for the single-component RA_g process, the second moments $M_{k,\ell}$ $(k+\ell\geqslant 2)$ exhibit strong fluctuations after a gel transition. In Fig. 10, we present time series for the average moments $M_{0,0}$, $M_{0,2}$, $M_{1,1}$, and $M_{0,2}$ of gelling $(y,\lambda)=(0.4,0.2)$ and nongelling $(y,\lambda)=(0.4,0.5)$ processes computed from ten replicate simulations per (λ,y) pair. Here, we normalize the moments according to the physical limit for finite systems of particles,

$$\frac{[VM_{k,\ell}(t)]}{[VM_{1,0}(t)]^k[VM_{0,1}(t)]^\ell}\leqslant 1, \quad k+\ell\geqslant 2. \quad (53)$$

In Fig. 11, we present the corresponding coefficients of variation. Like the second moments of the single-component RA_g process, the "second" moments $M_{0,2}$, $M_{1,1}$, and $M_{0,2}$

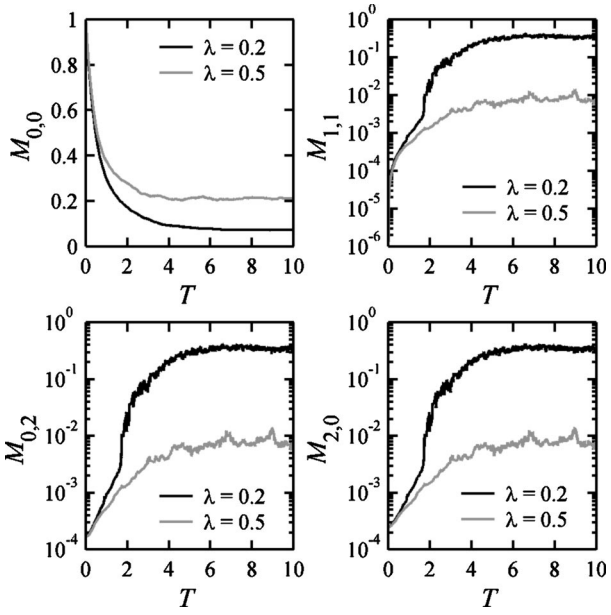

FIG. 10. Average moments of the RA_4/RB_2 composition distribution with λ above and below the gelation threshold and relative RA_4 monomer content $y=0.4$. In processes with $\lambda=0.2$, a gel transition is observed, resulting in a rapid and sizable jump in the second-order moments.

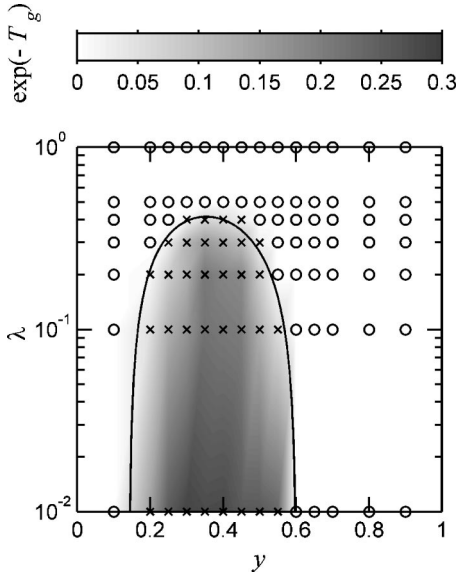

FIG. 12. Phase diagram for the RA_4/RB_2 polymerization process. λ is the dimensionless dissociation constant and y is the ratio of RA_4 monomers to total reactive monomers. Crosses denote polymerizations featuring a gel transition. Polymerizations lacking a gel transition are represented by circles. Gel points are indicated in the shading bar.

rapidly increase when the gel transition occurs. Moreover, the coefficients of variation of these moments go through unambiguous maxima for processes featuring a gel transition and exceed unity, whereas nongelling processes increase monotonically to asymptotic values smaller than 1. In some cases, nongelling processes appeared to have coefficients of variation in excess of 1. However, these were invariably consequences of artificial fluctuations as discussed in the preceding section when the asymptotic limit of a coefficient of variation was close to 1. Moreover, the noise of the second moments as computed from the individual simulations was invariably Brownian for nongelling processes and colored for gelling ones, in analogy with the results for the single-component RA_g polymerization (data not shown).

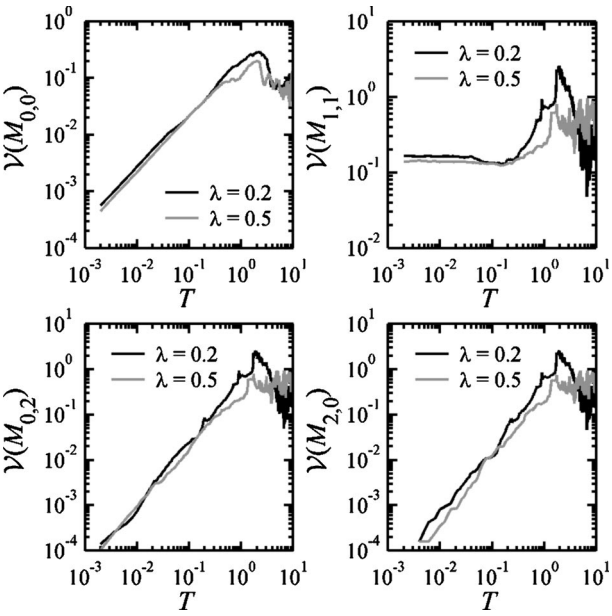

FIG. 11. Coefficients of variation of moments of the RA_4/RB_2 composition distributions with dissociation constants in the gelling and nongelling regions. In processes featuring a gel transition, $\mathcal{V}(M_2)$ has a peak in excess of unity, reflecting strong fluctuations in the composition distribution at the gel point.

Organizing the results of thousands of replicate simulations over the (λ,y) space, we constructed a phase diagram for the RA_4/RB_2 process (Fig. 12). In this figure, circles denote simulations that featured no gelation and squares denote simulations in which gelation occurred. The shading indicates the magnitudes of the gel points. As discussed in the preceding section, these are defined as the points in time where the simulation averaged values of $M_{0,0}$ are equal to

$$M_c = M_{0,0}(q_c), \tag{54}$$

as computed using Eq. (48) with q_c defined by Eq. (50). For every simulation in which a gel transition occurred, a macroparticle was generated in the species vector, the coefficients of variation of the second moments went through a peak in time, and the conversion q exceeded the critical value specified by Eq. (50). The converse was also observed. Processes that did not produce macroparticles featured monotonically increasing coefficients of variation of the second moments and their equilibrium conversions $q(\infty)$ were always smaller than q_c.

The additional curve shown in Fig. 12 is a deterministic prediction of the phase boundary, derived by extension of the method of van Dongen and Ernst to the chemistry of Eq. (23),

$$\lambda_c = \left(\frac{2r}{2r+g}\right)\frac{g(1-q_c)\left(\frac{1}{r}-q_c\right)}{q_c}. \tag{55}$$

The differences between the stochastic predictions of the phase boundary and Eq. (55) were negligible for almost all $\lambda > \lambda_c$, with some exceptions. In these cases, the neglect of the critical limit $q_{\max} = (yg)^{-1}$ in the deterministic method resulted in unreliable results for q_∞. Despite this, Eq. (55) is generally predictive of the gel transition. However, in analogy to our results for the single-component RA_g process, the time dependence of q predicted by Ziff's method was not accurate for $\lambda < \lambda_c$ and produced incorrect estimates of t_g for all λ and y.

The analysis used here to characterize the RA_4/RB_2 copolymerization may further the understanding of antibody agglutination. For a known dissociation constant ($K_D = k_2/k_1$) of an antibody-antigen pair, one can predict whether or not a mixture of the two molecules will result in a precipitate and when the precipitate will form. Copolymerizations of pertinence to immunology such as those of IgM ($g = 10$) with bifunctional antigens may be simulated and characterized likewise. However, the following caveats should be noted before applying these results. First, we have assumed that the internal cyclization is forbidden, which may not be true in a real agglutination process. Second, our analysis additionally presumes that there is no steric hindrance. Finally, the kernels we have used did not explicitly account for the effects of transport or Brownian motion, which may become important in the limit of gelation.

V. DISCUSSION

We have presented a simulation algorithm for determining the stochastic time evolution of reversibly aggregating systems of particles with multiple components or conservation laws. Because the simulation algorithm addresses aggregation and fragmentation events as random events, complex population balance equations may be replaced with simpler probability distributions that are amenable to Monte Carlo sampling. The simulation procedure first involves selection of a time interval τ in which no aggregation or fragmentation events occur. Subsequently, the imminent event is chosen—be it an aggregation of two particles or a fragmentation of a single particle. Finally, a time counter and the system state are updated to account for the consumption or production of particles. By successive selections of events and quiescence times, any virtual system of aggregating or fragmenting particles, biological cells, or molecules may be evolved stepwise, including those having time-dependent aggregation and fragmentation kernels. At the heart of this algorithm is the aggregation table—a data structure designed to keep track of multicomponent or multiproperty species and the probability densities of imminent events. The aggregation table accounts for aggregate species rather than individual particles, reducing the data storage requirements and increasing the speed by orders of magnitude.

We have applied the algorithm to three aggregation processes: the single-component RA_g polymerization, the single-component ARB polymerization, and the two-component RA_g/RB_2 copolymerization. The first of these is an aggregation of monomers featuring g functional groups that bind to identical functional groups on other monomers according to the chemical reaction $A + A \rightleftarrows A—A$. The latter two are mediated by the complexation reaction $A + B \rightleftarrows A—B$; the ARB process featuring one type of monomer with both types of functional group and the RA_g/RB_2 copolymerization featuring two types of monomers—one with g A ligands and the other with two B ligands. We examined statistical fluctuations during and following gel transitions of reversibly aggregating systems. The stochastically generated time series of the moments of size and composition distributions have different types of noise depending on the occurrence of a gel transition. Finally, we developed the first phase diagram to predict the gel transition for the RA_4/RB_2 copolymerization process in terms of its chemical properties. Using the stochastic simulation algorithm, the type of analyses performed for these processes may be applied to related biological processes such as the cross linking of cells via polyvalent or bivalent macromolecules. Specific examples include von Willebrand factor or fibrinogen-mediated platelet aggregation and the antibody-mediated cross linking of red blood cells in blood typing.

In this work, we have simulated processes for which (1) the aggregation and fragmentation kernels were related by the combinatorics of connecting multivalent monomers, and (2) aggregate formation was mediated by the formation of chemical bonds. However, many aggregation-fragmentation processes feature other mechanisms of aggregation and fragmentation, which are not microscopically reversible. Indeed, the steady states of such processes may not even be true equilibrium states. However, these issues are irrelevant to both the stochastic simulation algorithm and to the PBE so long as the forms of $K(\mathbf{u},\mathbf{v})$ and $F(\mathbf{u},\mathbf{v})$ correctly quantify the average rates of aggregation and fragmentation. Because the probability density functions underlying the algorithm are independent of the functional forms of the kernels, the stochastic simulation algorithm, like the PBE, can predict the time evolution of any process characterized by any pair of kernels $K(\mathbf{u},\mathbf{v})$ and $F(\mathbf{u},\mathbf{v})$.

In both this paper and in a previous publication [12], we have shown that the stochastic simulation algorithm can predict the time evolution of processes that feature a gel transition. Under certain conditions, processes described by ''shattering'' kernels are also amenable to simulation. However, this requires careful consideration of the size and composition space. When size or composition is treated as a continuous variable ($\mathbf{u} \in \mathbb{R}^\kappa$), solutions of the corresponding ''continuous'' PBE with certain fragmentation kernels imply a loss of system mass [27–29]. These results follow from the fact that particles are considered to be infinitely divisible. Thus, the ''shattering transition'' results from the disintegration of particles into infinitesimally small fragments. However, when particles are aggregates of monomeric units ($\mathbf{u} \in \mathbb{N}^\kappa$), the smallest particles must be monomers. Hence, solutions of a discrete PBE such as Eq. (3) with a ''shattering kernel'' will predict a rapid fragmentation of particles into

the constituent monomers. Because the stochastic simulation algorithm is indifferent to the functional forms of simulated kernels, it may be used to predict the time evolution of both ''aggregation dominated'' and ''fragmentation dominated'' processes with multiple components as long as the initial particles are composed of monomers.

APPENDIX

The maximum number of operations necessary for determining the composition of a daughter fragment in Eq. (22) follows from a consideration of the breakup of the aggregate of all particles in the system. Consider a system of particles composed of κ components, such as different types of chemical monomers or different blood cell types. Let us define $\Omega_k (k \in [1,\kappa])$ as the amount of each type of component particle. The number of distinct fragmentation kernels for the aggregate of all of the particles is then

$$\mathcal{N} = \prod_{k=1}^{\kappa} \left[\frac{1}{2} \Omega_k \right], \tag{A1}$$

where $[\frac{1}{2}\Omega_k]$ is the greatest integer less than $\frac{1}{2}\Omega_k$. Using the relationship between the amounts of each component and the maximum number of species $N_{\max}$ [12],

$$\prod_{k=1}^{\kappa} \Omega_k \simeq 2^{-\kappa} N_{\max}^{\kappa+1}, \tag{A2}$$

Eq. (A1) may be simplified to

$$\mathcal{N} \simeq N_{\max}^{\kappa+1}. \tag{A3}$$

If Eq. (22) is solved by bisection to obtain the composition of a daughter fragment, at most $\log_2(\mathcal{N})$ operations are required, for a maximum of $O(\ln(N_{\max}))$ operations. This does not include the the N operations necessary to specify the mother species.

[1] M.v. Smoluchowski, Z. Phys. Chem. **92**, 129 (1917).
[2] P.J. Blatz and A.V. Tobolsky, J. Phys. Chem. **49**, 77 (1945).
[3] A.A. Lushnikov, J. Colloid Interface Sci. **54**, 94 (1976).
[4] J.B. McLeod, Quart. J. Math. Oxford. **2**, 119 (1962).
[5] A.M. Golovin, Izv. Akad. Nauk SSSR, Ser. Geogr. Geofiz. **5**, 482 (1963).
[6] W. T. Scott, DRI Technical Report 9, 1965 (unpublished).
[7] F. Leyvraz and H.R. Tschudi, J. Phys. A **14**, 3389 (1981).
[8] P.L. Krapivsky and E. Ben-Naim, Phys. Rev. E **53**, 291 (1996).
[9] R.D. Vigil, R.M. Ziff, and B.L. Lu, Phys. Rev. B **38**, 942 (1988).
[10] M.H. Bayewitz, J. Yerushalmi, S. Katz, and R. Shinnar, J. Atmos. Sci. **31**, 1604 (1974).
[11] A.A. Lushnikov, J. Colloid Interface Sci. **65**, 276 (1978).
[12] I.J. Laurenzi, J.D. Bartels, and S.L. Diamond, J. Comput. Phys. **177**, 418 (2002).
[13] D.T. Gillespie, J. Atmos. Sci. **29**, 1496 (1972).
[14] D.T. Gillespie, J. Atmos. Sci. **32**, 1977 (1975).
[15] E.M. Hendriks, J.L. Spouge, M. Eibl, and M. Schreckenberg, Z. Phys. B: Condens. Matter **58**, 219 (1985).
[16] J.L. Spouge, J. Colloid Interface Sci. **107**, 38 (1985).
[17] M. Thorn, H.P. Breuer, F. Petruccione, and J. Honerkamp, Macromol. Chem. Theory. Simul. **3**, 585 (1994).
[18] M. Thorn and M. Seesselberg, Phys. Rev. Lett. **72**, 3622 (1994).
[19] I.J. Laurenzi and S.L. Diamond, Biophys. J. **77**, 1733 (1999).
[20] K. Lee and T. Matsoukas, Powder Technol. **110**, 82 (2000).
[21] D.T. Gillespie, J. Comput. Phys. **22**, 304 (1976).
[22] W.H. Stockmayer, J. Chem. Phys. **11**, 45 (1943).
[23] R.M. Ziff, J. Stat. Phys. **23**, 241 (1980).
[24] P.G.D. van Dongen and M.H. Ernst, J. Stat. Phys. **37**, 301 (1984).
[25] D.A. McQuarrie, C.J. Jachimowski, and M.E. Russell, J. Chem. Phys. **40**, 2914 (1964).
[26] I.G. Darvey, B.W. Ninham, and P.J. Staff, J. Chem. Phys. **45**, 2145 (1966).
[27] A.F. Filippov, Theor. Probab. Appl. **4**, 275 (1961).
[28] E.D. McGrady and R.M. Ziff, Phys. Rev. Lett. **58**, 892 (1987).
[29] R.D. Vigil and R.M. Ziff, J. Colloid Interface Sci. **133**, 257 (1989).